AD-A190 793 DEFORMATION OF RAPIDLY SOLIDIFIED DISPERSION STRENGTHENED TITANIUM ALLOYS(U) PENNSYLVANIA STATE UNIV UNIVERSITY PARK DEPT OF MATERIALS SCI.. 1/1

UNCLASSIFIED S L KAMPE ET AL. DEC 87 TR-8 F/G 11/6.1 NL

END
DATE
FILMED
5 88

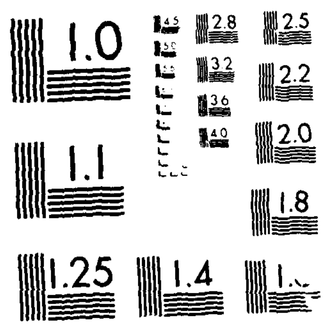

MICROCOPY RESOLUTION TEST CHART
NATIONAL BUREAU OF STANDARDS 1963-A

(4)

TECHNICAL REPORT NO. 8

TO

THE OFFICE OF NAVAL RESEARCH
CONTRACT NO. N00014-86-K-0381

DEFORMATION OF RAPIDLY SOLIDIFIED DISPERSION STRENGTHENED TITANIUM ALLOYS

S. L. Kampe+ and D. A. Koss*

+ Department of Metallurgical Engineering
Michigan Technological University
Houghton, MI 49931

Currently: Martin Marietta Laboratories
1450 S. Rolling Rd.
Baltimore, MD 21227

* Department of Materials Science and Engineering
The Pennsylvania State University
University Park, PA 16802

REPORT DOCUMENTATION PAGE

READ INSTRUCTIONS BEFORE COMPLETING FORM

1. REPORT NUMBER
No. 8

2. GOVT ACCESSION NO.

3. RECIPIENT'S CATALOG NUMBER

4. TITLE (and Subtitle)
Deformation of Rapidly Solidified Dispersion Strengthened Titanium Alloys

5. TYPE OF REPORT & PERIOD COVERED

6. PERFORMING ORG. REPORT NUMBER

7. AUTHOR(s)
S. L. Kampe and D. A. Koss

8. CONTRACT OR GRANT NUMBER(s)
N00014-86-K-0381

9. PERFORMING ORGANIZATION NAME AND ADDRESS
Department of Materials Science and Engineering
The Pennsylvania State University
University Park, PA 16802

10. PROGRAM ELEMENT, PROJECT, TASK AREA & WORK UNIT NUMBERS

11. CONTROLLING OFFICE NAME AND ADDRESS
Office of Naval Research
800 N. Quincy Street
Arlington, VA 22217

12. REPORT DATE
December 1987

13. NUMBER OF PAGES
34

14. MONITORING AGENCY NAME & ADDRESS (if different from Controlling Office)

15. SECURITY CLASS. (of this report)
unclassified

15a. DECLASSIFICATION/DOWNGRADING SCHEDULE

16. DISTRIBUTION STATEMENT (of this Report)
Distribution of this document is unlimited

17. DISTRIBUTION STATEMENT (of the abstract entered in Block 20, if different from Report)

18. SUPPLEMENTARY NOTES

19. KEY WORDS (Continue on reverse side if necessary and identify by block number)
Deformation, Creep, Rapidly Solidification, Dispersion Strengthening, Titanium Alloys

20. ABSTRACT (Continue on reverse side if necessary and identify by block number)

The influence of erbium on the flow behavior of titanium and titanium-aluminum base alloys has been investigated over a range of strain rates and temperatures (25° - 775°C). Data from as hot-extruded bulk specimens indicate that, although oxide dispersion strengthening can be large under certain conditions, the strengthening is minimal in fine-grain material subjected to low strain-rate deformation at high temperatures. Both micro-structural observations and an analysis of the flow data indicate profuse

20. con't.

grain boundary sliding under these conditions. Grain coarsening anneals, which also coarsen the dispersoids and increase their population along grain boundaries, result in significantly improved high temperature flow strengths, especially in the high temperature/low strain-rate regime.

(Kayser L.A

Accession For	
NTIS GRA&I	X
DTIC TAB	☐
Unannounced	☐
Justification	
By	
Distribution/	
Availability Codes	
Dist	Avail and/or Special
A-1	

QUALITY INSPECTED 2

DEFORMATION OF RAPIDLY SOLIDIFIED DISPERSION STRENGTHENED TITANIUM ALLOYS

S. L. Kampe+ and D. A. Koss*

+ Department of Metallurgical Engineering
Michigan Technological University
Houghton, MI 49931

Currently: Martin Marietta Laboratories
1450 S. Rolling Rd.
Baltimore, MD 21227

* Department of Materials Science and Engineering
The Pennsylvania State University
University Park, PA 16802

ABSTRACT

The influence of erbium on the behavior of titanium- and titanium-aluminum base alloys has been investigated over a range of strain rates and temperatures (25° - 775°C). Data from as hot-extruded bulk specimens indicate that, although oxide dispersion strengthening can be large under certain conditions, the strengthening is minimal in fine-grain material subjected to low strain-rate deformation at high temperatures. Both microstructural observations and an analysis of the flow data indicate profuse grain boundary sliding under these conditions. Grain coarsening anneals, which also coarsen the dispersoids and increase their population along grain boundaries, result in significantly improved high temperature flow strengths, especially in the high temperature/low strain-rate regime.

INTRODUCTION

OXIDE DISPERSON STRENGTHENING (ODS) of titanium-based alloys creates the potential of a new generation of lightweight, high-performance alloys with improved strengths and creep properties at elevated temperatures. The improvements in mechanical performance have been attributed to the presence of insoluble oxide particles which act as barriers to dislocation motion and remain microstructurally stable even to high temperatures. A principal difficulty encountered in the development of ODS alloys is the need for a processing technique capable of creating a uniform distribution of finely spaced, insoluble particles. However, the recent application of rapid solidification (RS) techniques to titanium-based alloys have indicated the potential to obtain oxide particle dispersoids distributed homogeneously within the matrix. These alloys utilize rare earth elemental additions to titanium because of their ability to scavenge interstitial oxygen from titanium solid solution and form a dispersion of thermally stable rare earth oxide precipitates.

Several investigators have established the potential of RS in oxide dispersion strengthened titanium alloy development through extensive evaluation of the thermal stability of candidate microstructures in the unconsolidated form of ribbon, flake, or splats (see, for example REF 1-11). The evaluation of the thermal stability following consolidation and the resulting bulk mechanical properties has progressed to a much lesser extent, however. Sastry, Peng, and Beckerman have measured the tensile strengths and steady state creep rate of extruded RS Ti, Ti-1.0Er, and Ti-1.5 Nd at two levels of stress for temperatures of 482, 600, and 700°C.[12] These data show decreased steady-state creep rates for the dispersoid-containing alloys with the Ti-Er alloy exhibiting superior creep resistance. Gigliotti et. al. have very recently reported the minimum creep rate and creep ductility at 650°C for several complex Ti alloys (containing varying amounts of Al, Sn, Zr and Nb) with erbium elemental additions. [13,14] In contrast, they report ductility improvements in alloys containing the rare-earth dispersoids but an associated loss of strength. Enhanced creep resistance with no compromise in ductility was obtained using rare-earth additions to titanium matrices of higher (Al + Sn) content. It should be noted that data reported by Sastry et.

al. for various RS Ti-Al alloys with rare earth additions have also demonstrated enhanced room temperature strength and ductility over non-dispersoid containing alloys. [15,16]

Although based on specific testing conditions, the above developmental work demonstrates the potential of RS processing techniques as a means of producing high-temperature titanium alloys. However, none of the above is aimed at establishing the controlling deformation mechanisms in fully processed bulk material. The present research reports strength and high temperature flow behavior over a much wider range of temperatures, strain-rates, and stresses than previously examined. It focuses on a range of alloy compositions based the technologically important Ti-Al system alloyed with elemental erbium and extends the previously reported results on the binary Ti-Er system. [17] Particular attention has been given to analyses of mechanisms of plastic flow at elevated temperatures, as well as the influence of microstructure especially matrix grain size, dispersoid size and distribution, on the observed behavior.

EXPERIMENTAL PROCEDURE

A. Material

Rapidly solidified Ti-2Er (all compositions in weight %) and Ti-6Al-2Er alloys were produced in ribbon form using a melt spinning apparatus as described elsewhere.[18] Rapidly solidified Ti-10Al, Ti-10Al-1Er, Ti-12Al, and Ti-12Al-1Er were also obtained in consolidated form; these alloys were produced using the pendant drop melt extraction (PDME) technique. [19] For comparison purposes, conventionally processed compacts of commercially pure (CP) titanium were also prepared and evaluated.

B. Consolidation Processing

The as-received melt-spun ribbon was consolidated into bulk form using a two-step procedure. The procedure involves hot isostatically pressing (HIP) under conditions of moderate consolidation temperature and high pressure (800°C/207MPa/4hr). Following HIP, the HIP cans were removed by machining and the alloys inserted into a protective stainless steel jacket for hot

extrusion at 750°C and a 7:1 reduction ratio. The protective jacket was removed from the extruded alloy bar by machining to final specimen diameter of 4.0 mm.

Right cylinder compression samples were machined directly from the as-extruded (RS alloys) or swaged (CP Ti) rod to a diameter of 4.0 mm and cut to lengths of approximately 10.7 mm. The ends of the compression pieces were polished parallel, and the sample surfaces were electropolished using an electrolytic solution of 10 v/o $HClO_3$ in methanol.

To avoid contamination of the titanium alloys during elevated temperature testing, a sealed atmosphere chamber was constructed to fit around the compression fixtures. The chamber was vacuum evacuated prior to testing and backfilled with high purity, flowing argon during testing. The test procedure included a 30 minute ramp-up time to the desired test temperature, followed by a one hour hold time. Actual temperature of the sample was monitored independent of the furnace controller using a thermocouple positioned in physical contact with the specimen. Temperature profiles along the length of the specimen indicated the hot zone of furnace was approximately eight times the length of the specimen; during testing, temperature fluctuations within the hot zone did not exceed ± 1°C.

Slow strain-rate compression testing was performed at temperatures of 20, 300, 600, 700 and 775°C. An extensometer attached to the compression fixtures enabled crosshead displacement to be accurately measured and recorded. Data was obtained by deforming at constant crosshead speed to 3.0% strain, and/or by strain-rate change tests at engineering strain rates of 5.0×10^{-5}, 2.5×10^{-4}, 1.25×10^{-3}, and 6.25×10^{-3} s^{-1}. In the latter case, the engineering strain rate was instantaneously changed from 5.0×10^{-5} to 2.5×10^{-4} s^{-1} at 3.0% strain, from 2.5×10^{-4} to 1.25×10^{-3} s^{-1} at 5.0% total strain, and from 1.2×10^{-3} to 6.25×10^{-3} s^{-1} at 7.0% total strain. The strain rate was also stepped down through a reverse sequence of the same values at total strains of 9.5, 11.5, 13.5%. These flow stress data showed no effect of strain on the steady state flow stresses measured, and the strain-rate sensitivity data obtained during strain-rate increases was the same as that obtained during the decreases. Strain rates were calculated using the predicted instantaneous height (based on the accumulated plastic strain) of the specimen at the time of the strain-rate

change. Following testing, true stresses before and after each strain-rate change were obtained graphically from the load-displacement plot using the procedure reviewed by Basinski, et. al.[20] After testing, the total plastic strain as determined from the final height of the test piece generally agreed well (within ±2%) with that predicted from the load-crosshead data; nonetheless a correction procedure used by Whittenberger[21] was applied to normalize the data with respect to the final measured height.

RESULTS AND DISCUSSION

A. Microstructural Evolution During Consolidation Processing

The microstructures which result following hot isostatic pressing show evidence of the prior ribbon boundaries as manifested by porosity and large erbia particles which accumulated along these boundaries.[22] Less conspicuous were occasional differences in grain size occurring across the prior ribbon boundaries. The difference in grain size can be attributed to variations in RS solidification parameters from ribbon to ribbon.

Fig. 1 shows the Ti-2Er alloy following 7:1 extrusion at 700°C. The prior-ribbon boundary features described above have been eliminated or dispersed to such an extent as to no longer delineate the prior ribbon boundaries. Additionally, dynamic recrystallization during extrusion has produced fine (approx. 4 μm) equiaxed grains.

Transmission electron micrographs (TEM) of the series of as-processed erbium-containing alloys following extrusion and a 775°C/2hr residual stress anneal are shown in Fig. 2. Evident in these micrographs are several features: (a) many fine dispersoids are present; these reside generally within the interior of the grains, (b) a few very large dispersoids are also present; these are usually located on the grain boundaries, (c) the very fine grain size (approx. 3-4 μm) of the titanium-rich matrix which has evolved during processing. Heat treatments of all alloys for times ≥ 12 hr at temperatures ~ 100°C below the respective beta transus temperatures indicate that these microstructural features are extremely stable; no discernable grain size or dispersoid coarsening occurs within the alpha-Ti microstructure.

TEM micrographs following high temperature anneals designed to increase the grain size are shown in Fig. 3 for the Ti-2Er, Ti-6Al-2Er, and Ti-10Al-1Er alloys (grain growth anneals for Ti-12Al-1Er were not performed). In addition to the approximate order of magnitude increase in grain size (to 25, 40, and 35 μm, respectively), the beta anneal has resulted in significant coarsening of the dispersoid particles. Based on measurements obtained from TEM micrographs, Figs. 4 and 5 are typical of the results of the dispersoid size distribution for the as-processed alloys, as well as for those subjected to the grain growth anneal. A summary of the heat treatments and the resulting average grain and dispersoid sizes is shown in Table I. As pointed out by Konitzer et. al. [7], the strain contrast associated with some of the very fine ($\leq$ 40 nm) dispersoids make accurate size measurements difficult. Even though the contrast was somewhat sensitive to orientation of the incident beam and could be minimized, it should be noted that the dimensions in this size range are approximate; these figures accurately represent the distribution of the dispersion in terms of size and number density.

Although the initial, as-processed dispersoid size is slightly larger in the aluminum-containing alloys, Figs 4 and 5 as well as Table I indicate that these alloys appear to be more resistant to dispersoid coarsening during the high temperature anneals, consistent with the results reported by Konitzer, et. al.[10] For example, the average dispersoid size with the beta-annealed Ti-2Er increased from 26 to 302 nm while those of the (Ti-6Al)-2Er increased only from 81 to 251 nm. In addition, both the Ti-6Al-2Er and Ti-10Al-1Er alloys show evidence of additional dispersoid formation during the grain growth anneal. This results in the bimodal particle size distribution in Figs. 4 and 5.

Also noted during the dispersoid measurements was the number fraction of dispersoids which reside on a grain boundary. In this regard, for each alloy in the as-processed condition, approximately one percent of the dispersoids were located at or very near a grain boundary. Following the grain growth anneals, this percentage increases in each case to greater than 12%, even though grain boundary area has decreased.

Recent quantitative microdiffraction analyses by Konitzer et. al. on RS Ti alloys have characterized in detail the erbia dispersion which evolves following heat treatment of supersaturated Ti-Er and Ti-Al-Er alloys.[7] These studies indicate a strong influence of both heat treatment temperature and time (which, in the present work includes consolidation processing conditions) as well as the erbium to oxygen ratio (Er/O) on the character and stoichiometry of the resulting erbia dispersion. Based on chemical analyses in the present work (see Table I for oxygen contents),a stoichiometric deficiency of oxygen exists in all alloys studied, suggesting the possibility of continued oxidation of elemental Er to erbia precipitates with continued heat treatment. Support for this argument is presented in the following section.

B. Mechanical Performance Evaluation

1. Yield stress

The dependence of yield stress on temperature and strain-rate is shown in Figs. 6-8, which include data for both the fine and coarse grained materials. As seen in the figures, the yield stresses of nearly all of the alloys decrease rapidly with temperature and are strongly strain-rate sensitive, especially at higher temperatures. However, the coarse-grain, dispersoid-containing alloys exhibit a much reduced temperature sensitivity of the yield stress. In all cases, the fine-grain variants exhibit superior strength at lower temperatures (≤400°C) compared to the coarse grain counterparts. In contrast, at elevated temperatures (≥700°C), the fine-grain Ti alloys strengthened with Er or Al possess inferior strength when compared to their coarse grained counterpart. No grain size effect is observed for the pure Ti at elevated temperatures for the conditions in the present study.

The large loss of strength with increasing temperature observed in these alloys is typical for systems where an interstitial solute has strong strengthening effects within the base alloy. In particular, the presence of oxygen, a potent solid solution strengthener of the hcp alpha-Ti, is believed responsible for the relatively high strengths at low temperatures (T≤400°C) in the present study. As the temperature is increased, however, the interstitial oxygen loses its effectiveness to

impede dislocation motion due to increasing influence from thermally-assisted dislocation motion, and/or due to increasing mobility of oxygen within the titanium matrix. At intermediate temperatures, the interstitial oxygen becomes completely ineffective as an obstacle to dislocation motion, and the yield stress becomes insensitive to temperature, as observed. It should be noted that aluminum alloying additions in the titanium matrix retain their effectiveness as a solid solution strengthener to high temperatures.

The 10-20% decrease in room temperature yield strength of Ti with the addition of 2 w/o erbium (Fig. 6) is readily understood by noting the above-mentioned scavenging or gettering effect of erbium for oxygen which occurs within the Ti matrix. As pointed out above, the formation of erbia dispersoid particles will reduce the room temperature matrix strength by reducing the concentration of oxygen in solid solution. Hence, any particle hardening due to the presence of the erbia dispersoids is more than offset by the loss of solid solution strengthening due to a reduced concentration of oxygen in the Ti matrix. This point has also been recognized by Sastry et. al. who have attempted to introduce fine particles of "externally oxidized" Er_2O_3 into the titanium matrix using RS techniques, thereby maintaining the low temperature strengthening afforded by the interstitial oxygen.[6] It is interesting to note that in the Ti-10Al alloy (Fig. 8), the addition of 1% Er has very little solid solution softening effect, possibly because of the small amount of erbium.

The large difference in room temperature strength between the fine and coarse-grained alloys which is observed in Figs. 6 and 8 (but not in Ti-6Al-2Er, Fig. 7) is probably a result of three factors: (a) grain size strengthening, (b) dispersoid coarsening, and (c) depletion of matrix oxygen with additional internal oxidation of erbium to Er_2O_3. In addition to the expected Hall-Petch type grain size strengthening, a significant increase in interparticle spacing is evident by comparing Figs. 2 and 3; both of these factors would result in decreased strengths in the coarse-grain material. Also, additional Er_2O_3 precipitation during the prolonged, high temperature grain growth anneals has been inferred by Konitzer et. al. [7] and in the present particle size data. The

additional particle hardening from the fine-scale dispersoids is consistent with the observed improved strength retention of the erbium-containing alloys.

The relative insensitivity of the yield strength to temperature in the coarse-grain alloys strongly suggest that the microstructural strengthening has little dependence on interstitial oxygen. This is consistent with the likelihood that nearly all of the oxygen has been effectively gettered after the high temperature beta anneal coarsens existing dispersoids as well as nucleating and grows new ones. Strengthening contributions from an increased population of the thermally stable erbia dispersoids promote strength retention to higher temperatures which is especially pronounced in the Ti-6Al-2Er alloy (Fig. 7).

At the high test temperatures ($\geq$700° C), the yield stress begins to drop rapidly with temperature and is strongly strain-rate sensitive. In this temperature regime, time-dependent deformation mechanisms become increasingly operative. These mechanisms will be discussed in more detail in the following section.

2. Elevated temperature deformation

The results of the high temperature deformation testing over a range of strain rates are shown in Figs. 8 and 9 plotted in the general format originally introduced by Mukherjee, Bird, and Dorn. [23] The behavior of Ti-12Al and Ti-12A-1Er is very similar to the Ti-10Al alloys shown in Fig. 9. The exponential dependence of creep rate $\dot{\varepsilon}$ on stress σ (i.e., for $\dot{\varepsilon} \; \alpha \; \sigma^n$) is obtained from the slope of the data plotted in this fashion. The value of the stress exponent n has been used previously to identify specific creep-type deformation mechanisms. In the Figs. 9 and 10, the diffusion-compensated strain rate is shown as a function of modulus-compensated flow stress. Both the diffusion coefficient [24] and the elastic modulus [26,27] have been corrected for temperature. In all cases, the coefficient of self-diffusion for CP Ti has been used.[25] The stresses reported in these figures reflect the condition of zero work hardening associated with a specific strain rate and temperature. As demonstrated by Mecking, [28] these stresses represent "near" steady-rate stress and strain-rate values. Specifically, these diagrams represent a compilation of data for each alloy and grain size tested for tests at 600, 700, and 775°C.

Fig. 9a illustrates the results for CP Ti and Ti-2Er at grain sizes of 4 and 25 μm; these results have been discussed previously.[17] However, also included in the present figure are creep data reported by Sastry et. al.[12] for RS Ti and Ti-1.0 Er. These data show excellent agreement with the present results. Figs. 9b and 10 illustrate the results for the aluminum-containing Ti and Ti-Er alloys. In all cases, increasing the grain size results in significant improvements in creep resistance in the small stresses/low strain-rate regime. As in the case of Ti-2Er, each dispersion-strengthened alloy exhibits a "two-stage" deformation behavior, indicating that two deformation mechanisms are operative over the range of temperature, strain-rate, and stress imposed in the present study.

Fig. 11 illustrates the same data in Figs. 9 and 10, but presented in a manner so as to allow as comparison of the high temperature flow behavior of the alloys at roughly constant grain size. As seen by comparing binary alloy data in Figs. 9 and 10, increasing aluminum contents generally improve creep resistance. However, the influence of erbium additions is more complex and depends on grain size. The beneficial effect of the dispersoids in reducing the flow rate is much greater in the coarse-grain material, but that effect is quite sensitive to erbium content. While the addition of 2Er has a significant creep strengthening effect on pure Ti (especially in the coarse-grain condition), the presence of 1Er in the Ti-10Al and Ti-12Al alloys provides little or no strengthening. This indicates that there is a strong correlation of the higher erbium content with improved high temperature creep strength.

In order to understand the above behavior, certain results are pertinent: (1) the strong stress-sensitivity of the strain rate with a stress exponent which depends on grain size and the magnitude of the strain rate, (2) the strengthening effect of erbia dispersoids, especially in the coarse-grain alloys containing 2 Er, (3) the strong effect of grain size on flow stress, with the larger-grain material showing superior high temperature flow behavior particularly at low stresses/strain rates, and (4) the evidence of addition erbia precipitation during the grain-coarsening anneals. These results may be described using a general constitutive equation for high temperature creep behavior:

$$\dot{\varepsilon} = A\,(D_i/d^p)\,(\sigma/E)^n$$

where $\dot{\varepsilon}$ = strain rate, usually a steady state creep rate
- A = structure sensitive constant (independent of grain size)
- D_i = diffusion coefficient, with the subscript i referring to the operative diffusion mechanism
- d = grain size
- p = grain size exponent, usually 0, 1, 2, or 3 depending upon the operative deformation and/or diffusion mechanism
- σ = flow stress, usually a steady state flow stress
- E = elastic modulus
- n = stress exponent, a constant whose value is dependent on the deformation mechanism operative.

Thus for Dorn-type plots as in Figs. 9 and 10, A and n may be calculated respectively from the intercept and slope of the resulting curves. Additionally, because the value of the stress exponent n varies with and is dependent on the rate-controlling deformation mechanism, the resulting n- value can provide insight as to the mechanism of deformation over specific ranges of temperature, strain-rate, and stress.

As noted previously, each alloy strengthened with Al and/or Er exhibits two distinct deformation ranges as indicated by the two distinct values of stress exponent (n) over the range of temperature, strain-rate and stress studied (Figs. 9-11). For the conditions of high temperatures, low strain-rates/stresses, a small value of stress exponent is observed, specifically $n \sim 2\text{-}4$ in Figs. 9 and 10 as compared to a value of $n \geq 6$ observed at high strain rates/stresses. The small n-value occurs over the approximate range of temperature and strain-rates for which $\dot{\varepsilon}/D(T)$ is less than $10^{12}\ m^{-2}$. When coupled with the strong grain size effect, this small value of the stress exponent strongly suggests that grain boundary sliding is involved as a deformation mechanism under these conditions.

Table II illustrates various proposed constitutive equations for power law creep which would predict a stress exponent of $n \cong 2$ with a grain size exponent p of 2 or 3. [29] Each of these mechanisms involve grain boundary sliding (GBS) as a contributing deformation mechanism with the necessary concomitant continuum accommodation occurring via dislocation motion in adjacent

grains. Each of these mechanisms share a common phenomenological base, that is, the suggestion that an increment of GBS creates regions of high stress concentration along boundaries. In response, dislocations are emitted into adjacent grains along favored slip planes. Eventually, a backstress results from the dislocation pile-up, and continued steady-state deformation is limited by the rate at which dislocations can climb out of the slip plane. The equations differ by the specific nature of the climb process, i.e., whether climb of dislocations occurs within the gain boundary or within the bulk grain. In the former instance, the activation energy for the deformation process would be comparable to that for grain boundary diffusion, and lattice diffusion for the latter. It has also been proposed that pipe diffusion along dislocation cores can influence the rate of climb [30]. Unfortunately, grain size exponents of <u>both</u> 2 and 3 have been proposed for climb within the boundary.

Table III summarizes the calculated activation energies for creep in the present study for the high temperature, low strain-rate deformation conditions. As indicated, activation energies compare favorable to the value of 242 KJ/mol for lattice diffusion <u>and</u> power law creep reported by Sargent and Ashby, [25] as compared to 150 and 100 KJ/mol for grain boundary and dislocation pipe diffusion, respectively. Thus, these data indicate that lattice diffusion appears to be the rate controlling diffusion process for the slip-accommodated grain boundary sliding which is occurring in these alloys.

Fig. 12 illustrates the data for the Ti-Al and Ti-Al-Er alloys as compensated for an $\dot{\varepsilon} \alpha d^{-2}$ dependence of grain size*, and utilizing the coefficient for lattice self diffusion of titanium. As shown, the data for both grain sizes adjoin approximately along a single line for each alloy, affirming an approximate inverse-squared dependence of strain-rate on grain size. In addition, the calculated values of the constants for a constitutive equation in the form of Eq. 1 for each alloy have been summarized in Table IV. A comparison of these results to the models reviewed and

* These plots present data for which $\dot{\varepsilon}/D(T) \leq 10^{12}\ m^{-2}$. It should be noted that the authors have selected this value based entirely on the experimental data presented in Figs. 11 and 12 where it was noted that a change in mechanism occurs at <u>approximately</u> this value. Conceivably, this range may include data which reflects the transition between deformation mechanisms.

presented in Table II show that the grain size and stress exponents are in reasonable good agreement with those predicted for a micromechanism of GBS accommodated by slip and are also consistent with dislocation climb controlled by lattice diffusion (n≅2 and p=2). Of the alloys tested, however, the poorest correlation with the values listed in Table II are those for Ti-2Er and Ti-10Al; the resulting stress exponent value suggests no clear identification with a particular grain boundary sliding mechanism as listed in Table II. Nonetheless, noting the inverse dependence of the strain rate on the square of the grain size in <u>all</u> of the matrix-strengthened Ti alloys studied, we can reasonably conclude that some form of grain boundary sliding is the dominant high temperature deformation mechanism. This is consistent with TEM observations of grain boundary void deformation observed <u>only</u> under those stress/temperature/strain-rate conditions favoring grain boundary sliding.

It is worthwhile to point out that the proposed model of deformation in the present study is consistent and analogous to the "core and mantle' theory presented by Gifkins [31] for deformation under creep and/or superplastic conditions. This model suggests that GBS is accommodated by slip within a narrow 'mantle' encompassing the grain boundary and adjacent area; this surrounds a relatively rigid 'core'. Thus, steady state strain rate in a material deforming by GBS will be <u>decreased</u>, for example, by any microstructural change which acts to (1) decrease the ratio of grain boundary area to bulk crystal, thereby increasing the relative amount of deforming 'mantle', and/or (2) strengthen or introduces obstacles into the 'mantle' region, thus limiting the ability of the material to accommodate GBS by slip. In the present study, both conditions are satisfied with a commensurate decrease in strain rate following the high temperature grain growth anneals; grain size has increased thereby reducing the volume of 'mantle', and an increased volume of erbia resides on or near the grain boundaries, despite the large decrease in grain boundary area.

At higher strain-rates and stresses as well as low temperatures (and/or larger grain sizes), the deformation mechanism changes as is indicated by the change n the stress exponent under these imposed conditions of deformation (Fig. 11). Specifically, the stress exponents increase from n≅2 to n≥6, as summarized in Table V. In addition, post-deformation microscopy following

deformation at 600°C/1.25×10^{-3} s^{-1} (i.e. $\dot{\varepsilon}$ /D(T)=3×10^{13} m^{-2}) show evidence of extensive dislocation-particle interaction, with little evidence of grain boundary voiding (which was common after testing the fine grain material at the high temperature/low strain-rate regime). These observations and the value of stress exponent observed in this range suggests the following possible interpretations: (1) grain boundary siding no longer plays a major role in the deformation of these alloys, (2) that ODS-type deformation mechanisms have become solely operative, thus accounting for the apparent high stress exponents, [31] or (3) a breakdown of power law creep, as might be expected at these levels of stress. It is interesting to note that the grain-size effect observed under these conditions appears to be inconsistent with any of these models of deformation. The effect, which results in an increase in flow stress with an increase in grain size, is probably a consequence of the additional precipitation of erbia dispersoids which occur during the grain growth anneal as noted earlier and also proposed previously [7]. Support for this possibility is provided in the data for the Ti-10Al binary alloy (Fig. 9a), which does not show the "grain size effect" in the $\dot{\varepsilon}$ /D(T)$\geq 10^{12}$ m^{-2} deformation regime; obviously, no additional erbia precipitation could occur in this alloy during the beta anneal heat treatment.

Summary

When consolidated into bulk form, Ti-Er and Ti-Al-Er alloys produced by rapid solidification techniques retain a fine and homogeneous dispersion of oxide particles within fine-grain (3-5 μm) matrices. In the as-consolidated form, the majority of the dispersoids are very fine (average diameter ~ 40-80 nm) and generally reside within the interiors of the matrix grains. A few large dispersoids (diameter ≥ 200 nm) are also present; most of these are located on grain boundaries. Both the dispersoids and fine grains microstructure present in the as-processed alloys are extremely resistant to coarsening during high temperature anneals at temperatures near the beta-phase transus temperatures. An order-of-magnitude increase in grain size is achieved only by heat treatments at temperatures within the beta-phase field; however, this is accompanied by significant dispersoid coarsening and in some cases additional dispersoid formation.

Results from compression testing of the Ti, Ti-Er and Ti-Al-Er alloys over a range of temperatures (20° to 775°C) and strain rates ($5x10^{-5}$ to 6×10^{-3} s^{-1}) indicate that the yield and flow strength of these alloys is sensitive to temperature, strain rate, grain size, and alloy composition. For example, at room temperature the addition of erbium results in lower yield strengths; this is believed to be caused by a reduced solid solution strengthening component due to oxygen depletion as a result of the internal oxidation of the erbium to erbia. As the temperature is increased, oxygen loses its effectiveness as a strengthener; strength of these alloys at higher temperatures rely on contributions from aluminum in solid solution and particle strengthening from the stable oxide dispersoids.

Based on the conditions imposed in the present study, the high temperature deformation of these dispersion-strengthened titanium alloys is characterized by a "two stage" deformation behavior, which strongly suggests that two distinct deformation mechanisms are operative over the specific ranges of temperature, strain rates, and stresses. In the range of high temperatures and low stresses/strain rates ($\dot{\varepsilon}$ /D $\leq 1 \times 10^{12}$ m^{-2}), the mechanical test data and post-deformation microscopy indicate that grain boundary sliding is the rate-controlling deformation mechanism in the fine grain alloys. Increasing the grain size from 3-4 μm to 25-40 μm enhances the high temperature strength and creep resistance of the strengthened titanium alloys. This occurs as a result of (a) a minimization or elimination of grain boundary sliding as the dominant deformation mechanism due to the reduction of grain boundary area, (b) an increased density and size of dispersoids residing on grain boundaries, also acting to minimize grain boundary sliding by mechanically "pinning" the boundaries, and (c) additional precipitation of oxide particles which occur during the high temperature grain growth anneals, thus providing additional particle strengthening. The experimental behavior are in good agreement with constitutive equation which model deformation via grain boundary sliding mechanisms.

For low temperatures/high strain rates conditions the mechanical test data are consistent with a deformation mechanism of dislocation creep past obstacles. Post-deformation microscopy reveals evidence of significant dislocation-dispersoid interaction in alloys tested under these

conditions of temperature and strain rate ($\dot{\varepsilon}/D \geq 10^{12}\ m^{-2}$). The apparent grain size effect in the dispersoid-containing alloys under these conditions is interpreted to be a result of an increased population of dispersoids which evolve during the high temperature grain-growth anneals.

ACKNOWLEDGEMENTS

The authors wish to acknowledge valuable discussions with B. Pletka, materials supplied by R. Amato of General Electric, and assistance in consolidation processing by M. F. Gigliotti also of General Electric. The research was suppported by the Office of Naval Research through Contract N00014-86-K-0381.

REFERENCES

1. Processing of Structural Materials by Rapid Solidification (conf. proc.), ed. F. H. Froes and S. J. Savage, ASM, 1987).

2. F. H. Froes and R. G. Rowe: in Titanium Rapid Solidification Technology (proc. conf.), ed. F. H. Froes and D. Eylon, TMS-AIME, 1986, 1-19.

3. S. M. L. Sastry, P. J. Meschter, and J. E. O'Neal: Metall. Trans A, 1984, vol. 15A, 1451-63.

4. D. B. Snow and A. F. Giamei: in Titanium Rapid Solidification Processing (proc. conf.), ASM-AIME, 1986, 153-64.

5. S. H. Whang: J. Mater. Sci., 1986, vol. 21 (7), 2224-38.

6. S. M. L. Sastry, T. C. Peng, and J. E. O'Neal: in Titanium Science and Technology (proc. conf.), vol. 1, ed. G. Lutjering U. Zwicker, and W. Bunk, 1985, 397-404.

7. D. G. Konitzer, J. T. Stanley, M. H. Loretto, and H. L. Fraser: Acta Metall., 1986, vol. 34 (7), 1269-77.

8. F. H. Froes and R. G. Rowe: in Rapidly Solidified Alloys and Their Mechanical and Magnetic Properties (proc. conf.), ed. B. C. Giessen, D. Polk, and A. I. Taub, 1986, 309-334.

9. D. G. Konitzer and H. L. Fraser: in High Temperature Ordered Intermetallic Alloys (proc. conf.), ed. C. C. Koch, C. T. Liu, and N. S. Stoloff, MRS, 1985, 437-42.

10. D. G. Konitzer, B. C. Muddle, and H. L. Fraser: Scripta Metall., 1983, vol. 17, 1983, 963-66.

11. R. G. Rowe, T. F. Broderick, E. F. Koch=h, and F. H. Froes: in Rapidly Solidified Materials (proc. conf.), ed. P. W. Lee and R. S. Carbonara, 1985, 107-14.

12. S. M. L. Sastry, T. C.Peng, and L. P. Beckerman: Metall. Trans. A, 1984, vol. 15A, 1465-74.

13. M. F. X. Gigliotti, G. E. Wasielewski, and R. G. Rowe: in Titanium Rapid Solidification Technology (proc. conf.) ed. F. H Froes and D. Eylon, TMS-AIME, 1986, 141-51.

14. M. F. X. Gigliotti, R. G. Rowe, G. E. Wasiliewski, G. K. Scarr, and J. C. Williams: in Rapidly Solidified Alloys and Their Mechanical and Magnetic Properties (proc. conf.), ed. B. C. Giessen, D. R. Polk, and A. I. Taub, 1986, 343-50.

15. S. M. L. Sastry, T. C. Peng, and R. J. Lederich: in Mechanical Behavior of Rapidly Solidified Materials (proc. conf.), ed. S. M. L. Sastry and B. A. MacDonald, 1986, 231-45.

16. S. M. L. Sastry, D. M. Bowden, and L. D. Lederich: in Titanium Science and Technology (proc. conf.), vol. 1, ed. G. Lutjering, U. and W. Bunk, 1985, 435-41.

17. S. L. Kampe and D. A. Koss: in Processing of Structural Metals by Rapid Solidification (proc. conf.), ed. F. H. Froes and S. J. Savage, ASM, 1987, 175-80.

18. S. H. Whang: Rapidly Solidified Materials (proc. conf.), ed. P. W. Lee and R. S. Carbonara, 1985, 101-06.

19. S. J. Savage and F. H. Froes: J. Metals, 1984, vol. 36 (4), 20-33.

20. Z. S. Basinski, P. J. Jackson, and M. S. Duesbery: Phil. Mag., 1977, vol. 36 (2), 255-63.

21. J. D. Whittenberger: Metall. Trans. A, 1979, vol. 10A, 1285-95.

22. S. L. Kampe: Ph.D. Thesis, Michigan Technological University, 2987.

23. A. K. Mukherjee, J. E. Bird, and J. E. Dorn: Trans. ASM, 1969, vol. 62, 155-79.

24. M. Doner and H. Conrad: Metall. Trans. A, 1973, vol. 4, 2809-17.

25. P. M. Sargent and M. F. Ashby: Scripta Metall., 1982, vol. 16, 1415-22.

26. G. Simmons and H. Whang: Single Crystal Elastic Constants and Calculated Elastic Properties: A Handbook, 2nd Edition, M.I.T. Press, 1971, 324-25.

27. E. W. Collings: The Physical Metallurgy of Titanium Alloys, ASM, Metals Park, OH, 1984, 117.

28. H. Mecking: in Work Hardening in Tension and Fatigue (proc. conf.), ed. A. W. Thompson, 1977, 67-88.

29. B. Walser and O. D. Sherby: Scripta Metall., 1982, vol. 16, 213-19.

30. O. A. Ruano, A. K. Miller, and O. D. Sherby: Mat. Sci. Eng., 1981, vol. 51, 9-16.

31. R. C. Gifkins: Metall. Trans. A, 1976, vol. 7A, 1225-32.

32. J. K. Tien, T. E. Howson, and D. E. Matejczyk: in Frontiers of High Temperature Materials, ed. J. S. Benjamin, 1981, INCO, 13-22.

Table I. Summary of heat treatments and resulting average grain and dispersoid sizes

Alloy	Heat Treatment	Grain Size (μm)	Dispersoid diameter (nm)
CP Ti	775°C/2h	4	
CP Ti	800°C/4h	25	
Ti-2Er	775°C/2h	4	26
Ti-2Er	932°C/2h/775°C24h	25	302
Ti-6Al-2Er	775°C/2h	4	81
Ti-6Al-2Er	1050°C/1h/775°C/24h	40	251
Ti-10Al	775°C/2h	3	
Ti-10Al	1000°C/5h	35	
Ti-10Al-1Er	775°C/2h	3	70
Ti-10Al-1Er	1080°C/0.5h/775°C/24h	35	196
Ti-12Al	775°C/2h	3	
Ti-12Al-1Er	775°C/2h	3	62

Table II. Constitutive equations for slip-accommodated grain boundary sliding of metals [28]

Rate-limiting diffusion mechanism	Constitutive equation
Lattice	$\dot{\varepsilon} = 2 \times 10^9\ (D_L/d^2)\ (\sigma/E)^2$
Grain boundary	$\dot{\varepsilon} = 1 \times 10^8\ (D_B/d^3)\ (\sigma/E)^2$
Pipe (dislocation core)	$\dot{\varepsilon} = 2 \times 10^{11}\ D_p/d^2)\ (\sigma/E)^4$

Table III. Experimental activation energies for creep as calculated from the high temperature, low strain-rate/stress deformation data ($\dot{\varepsilon}/D(T) \leq 10^{12}\ m^{-2}$).

Alloy	Q_{creep} (KJ/mol)
CP Ti	273
Ti-2Er	246
Ti-6Al-2Er	244
Ti-10Al	186
Ti-10Al-1Er	246
Ti-12Al	201
Ti-12Al-1Er	270

Table IV. Constitutive equations which describe the data in the high temperature, low strain rate regime of deformation ($\dot{\varepsilon}/D \leq 10^{12}\ m^{-2}$), in the present study.

Alloy	Constitutive equation
Ti-2Er	$\dot{\varepsilon} = 6.0 \times 10^{11} (D_L/d^2)\ (\sigma/E)^{4.0}$
Ti-6Al-2Er	$\dot{\varepsilon} = 7.5 \times 10^{6} (D_L/d^2)\ (\sigma/E)^{2.2}$
Ti-10Al	$\dot{\varepsilon} = 6.0 \times 10^{8} (D_L/d^2)\ (\sigma/E)^{3.3}$
Ti-10Al-1Er	$\dot{\varepsilon} = 4.5 \times 10^{6} (D_L/d^2)\ (\sigma/E)^{2.3}$
Ti-12Al*	$\dot{\varepsilon} = 2.2 \times 10^{5} (D_L/d^2)\ (\sigma/E)^{2.0}$
Ti-12Al-1Er	$\dot{\varepsilon} = 2.0 \times 10^{6} (D_L/d^2)\ (\sigma/E)^{2.2}$

* Constants based on data from 1 grain size only.

Table V. Stress exponents for the present data in the lower temperature, higher strain rate regime of deformation ($\dot{\varepsilon}/D \geq 10^{12}$ m^{-2}).

Alloy	Grain Size (μm)	Stress Exponent
Ti	5 & 25	5.4
Ti-2Er	4	5.3
Ti-6Al-2Er	25	7.1
	40	14.9
Ti-10Al	3 & 35	8.8
Ti-10Al-1Er	3	14.8
	35	15.1
Ti-12Al	3	6.1
Ti-12Al-1Er	3	9.0

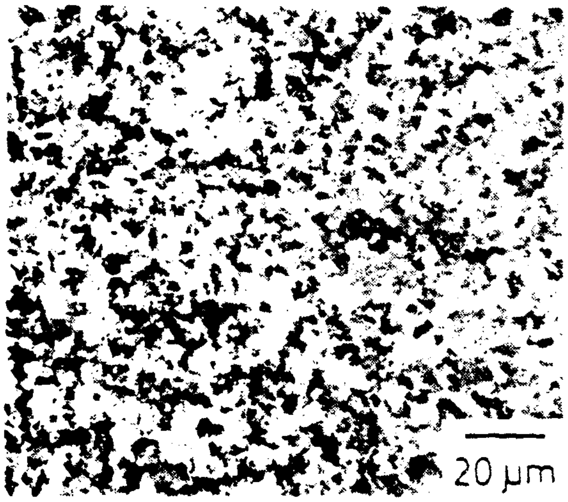

FIG. 1. Optical micrograph of the as-extruded Ti-2Er alloy illustrating the homogeneous, equiaxed grain structure which has evolved.

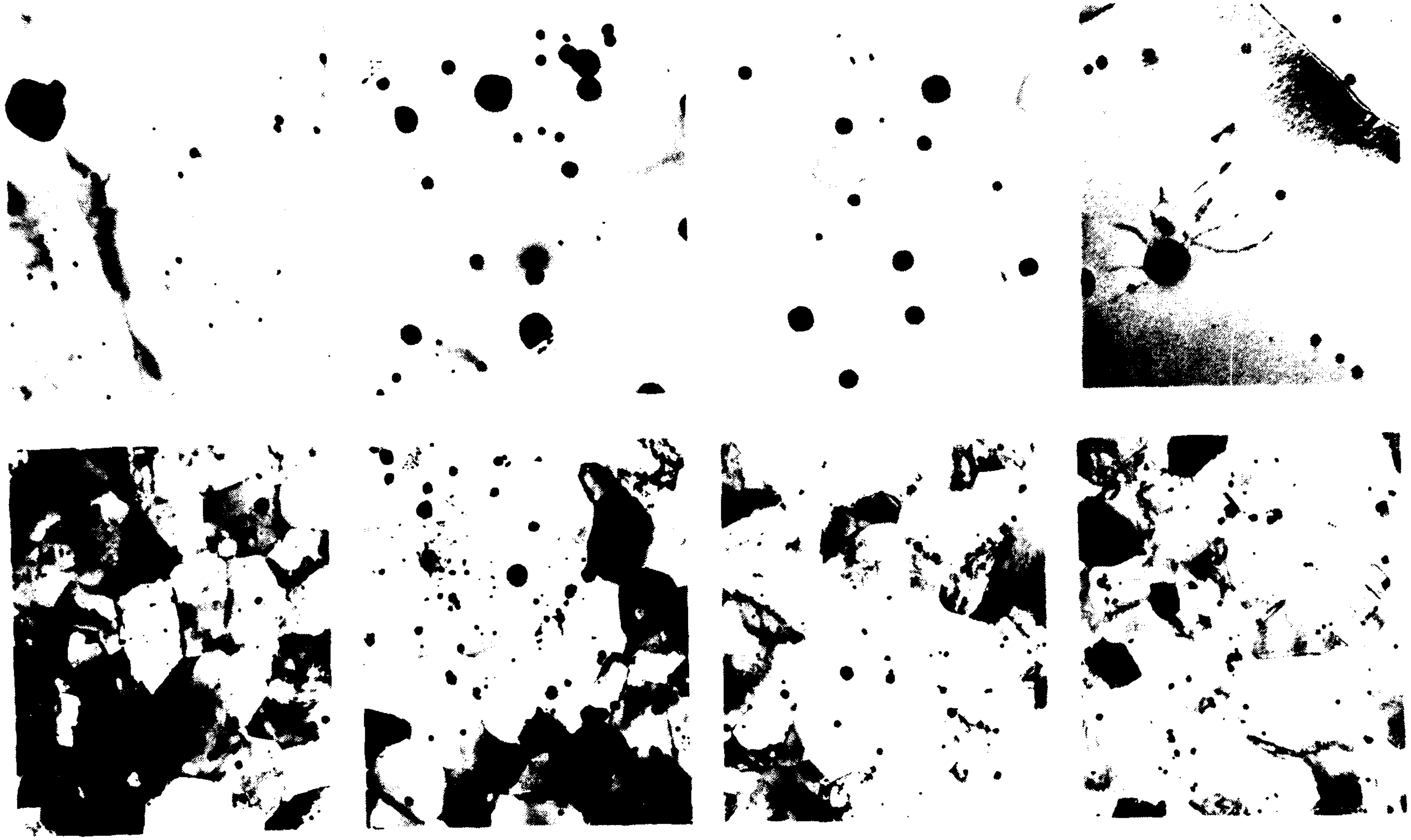

FIG. 2. TEM micrographs of the as-processed erbium-containing alloys following 775°C/2 h heat treatment: a.) T-2Er, b.) Ti-6Al-2Er, c.) Ti-10Al-1Er, and d.) Ti-12Al-1Er.

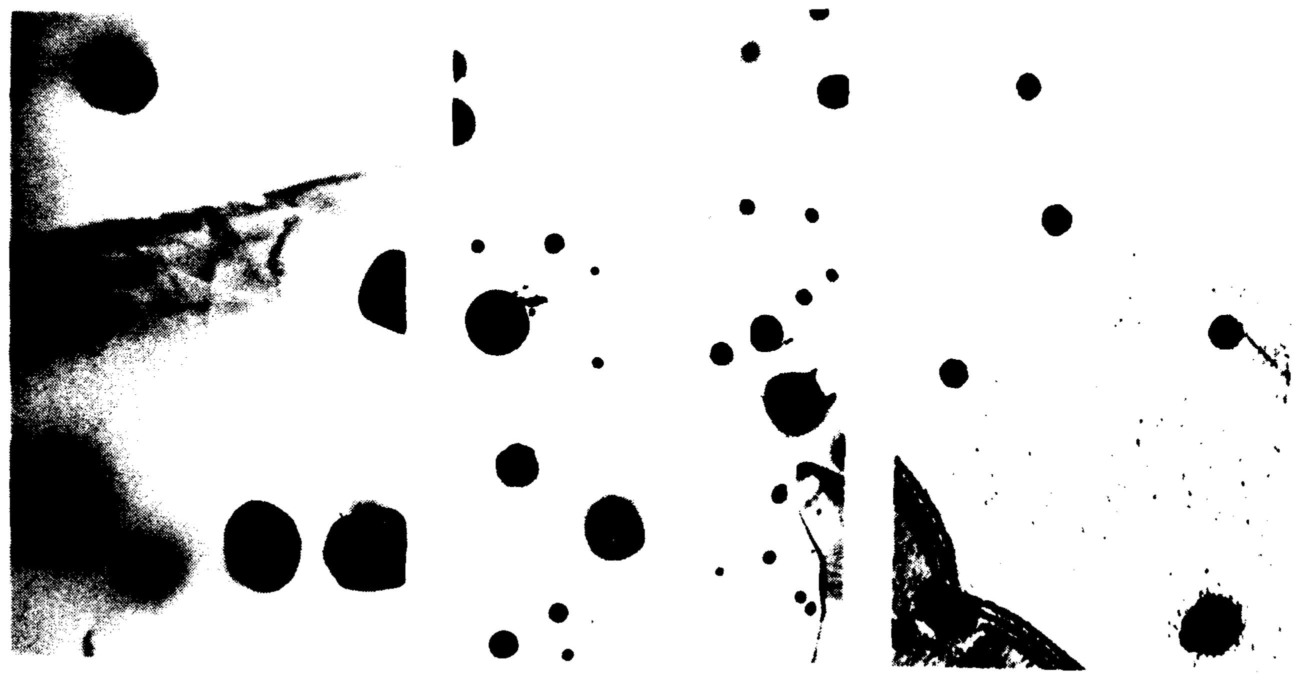

FIG. 3. TEM micrographs of the erbium-containing alloys following the grain growth anneals: a.) Ti-2Er, b.) Ti-6Al-2Er, and c.) Ti-10Al-1Er.

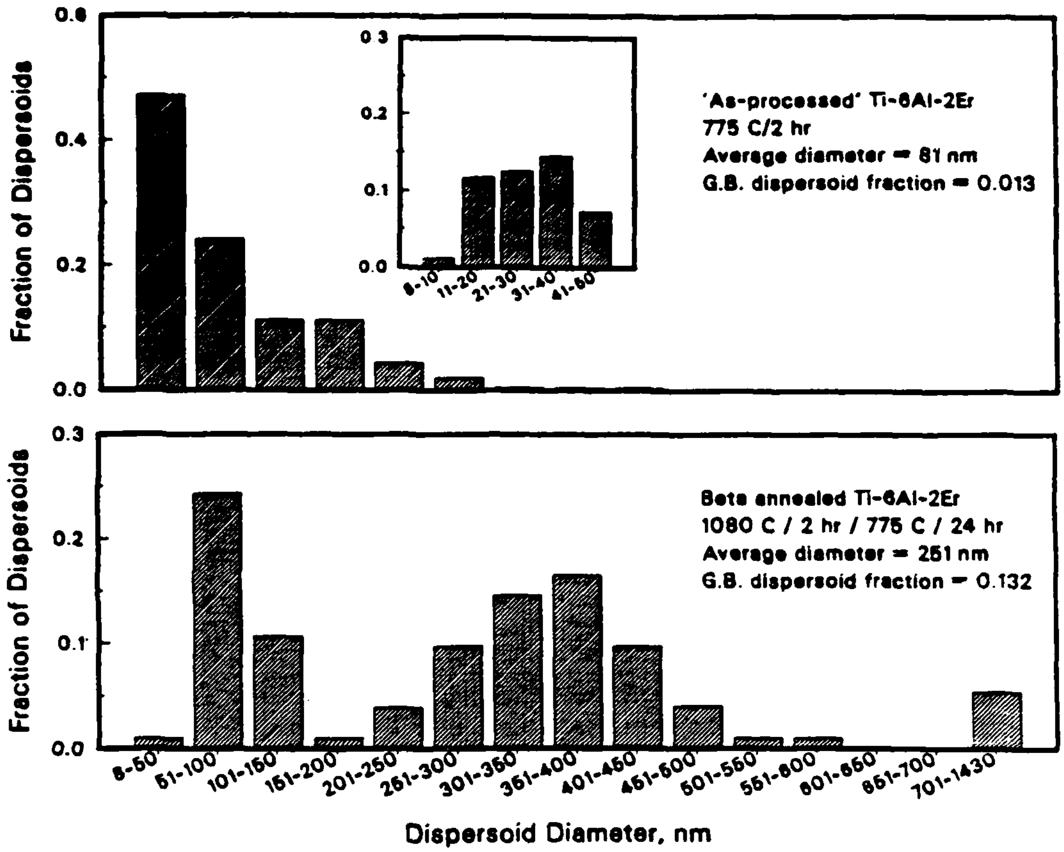

FIG. 4. Histograms illustrating the dispersoid size distribution for Ti-6Al-2Er: a.) in the as-processed condition, and b.) following the grain growth anneal.

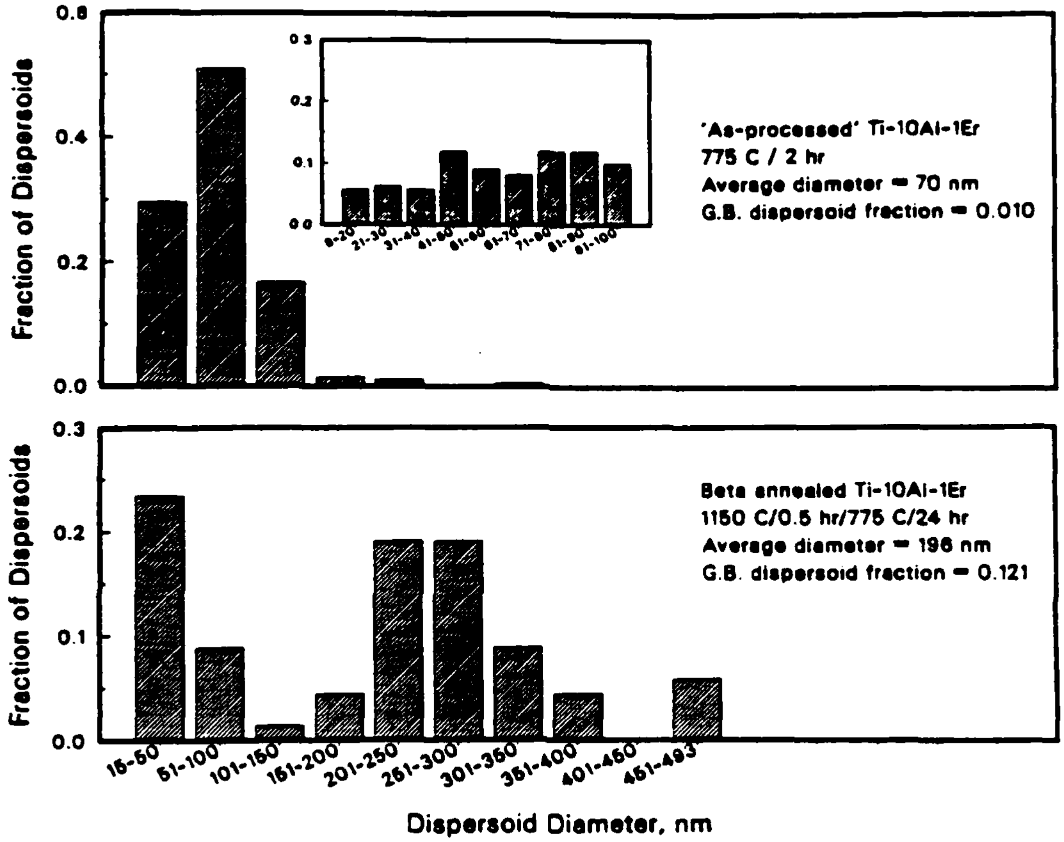

FIG. 5. Histograms illustrating the dispersoid size distribution for Ti-10Al-1Er: a.) in the as-processed condition, and b.) following the grain growth anneal.

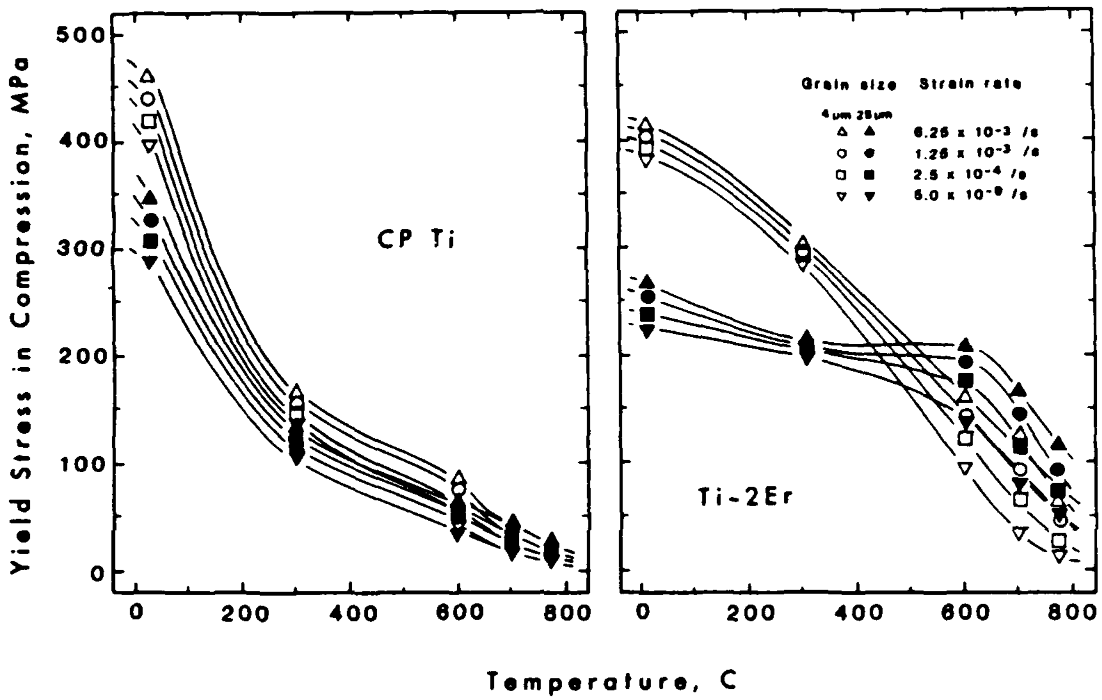

FIG. 6. The yield stress as a function of temperature and strain-rate for grain sizes of 4 and 25 μm for a.) CP Ti, and b.) Ti-2Er.

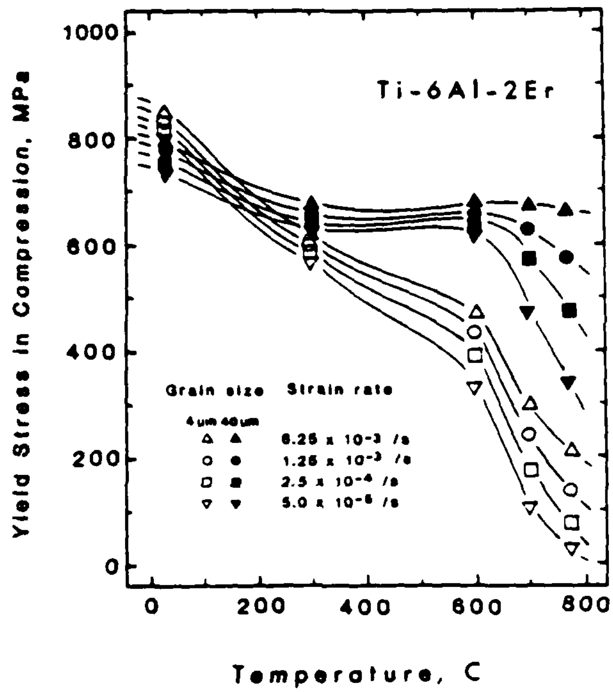

FIG. 7. The yield stress as a function of temperature and strain-rate for Ti-6Al-2Er with grain sizes of 4 and 40 μm.

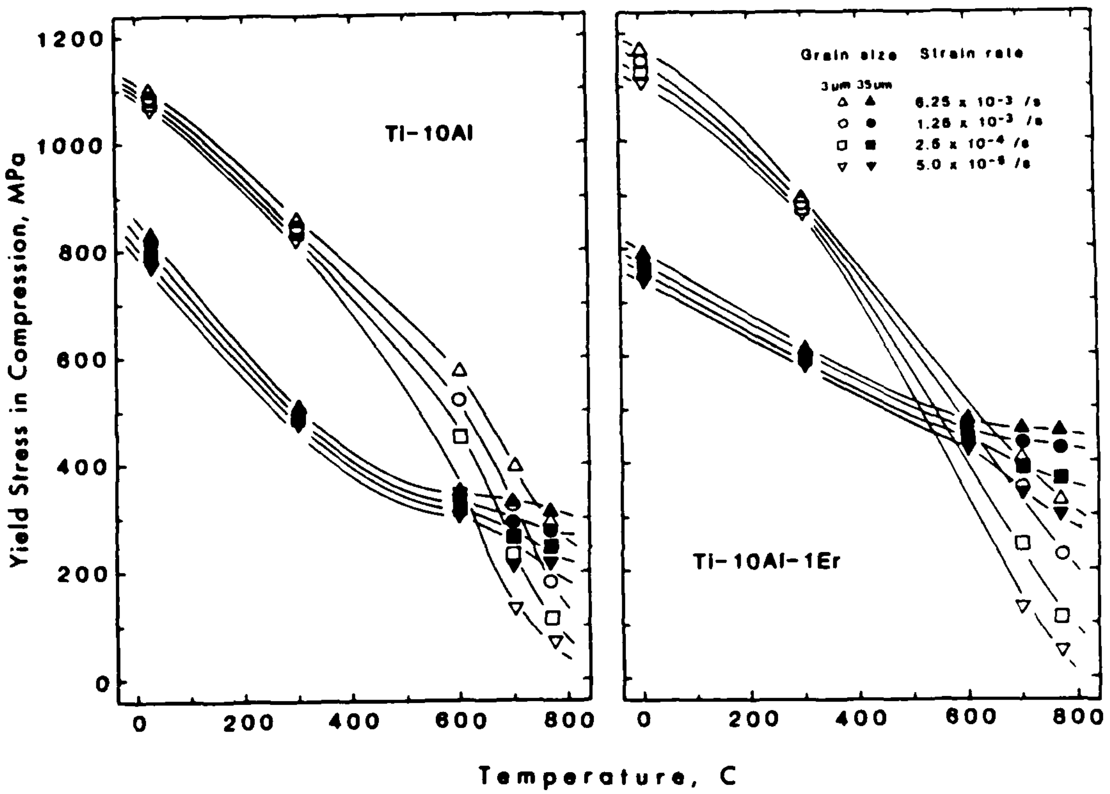

FIG. 8. The yield stress as a function of temperature and strain-rate for grain sizes of 3 and 35 μm for a.) Ti-10Al, and b.) Ti-10Al-1Er.

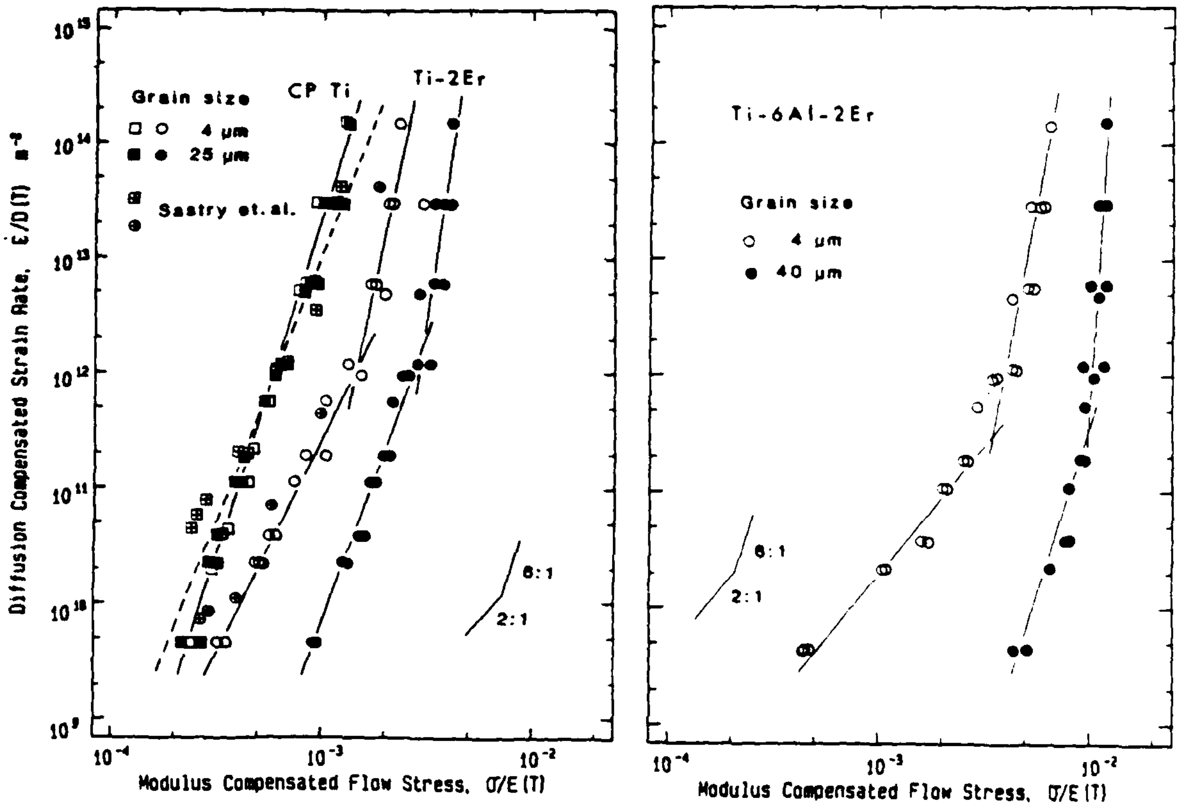

FIG. 9. Diffusion compensated near steady-state strain-rate as a function of modulus compensated flow stress for a.) CP Ti and Ti-2Er with grain sizes of 4 and 25 μm, and b.) Ti-6Al-2Er with grain sizes of 4 and 40 μm. Included in (a.) are data from Sastry et. al. [12] as well as the "best fit" Ti data (dashed line) from Doner and Conrad [24].

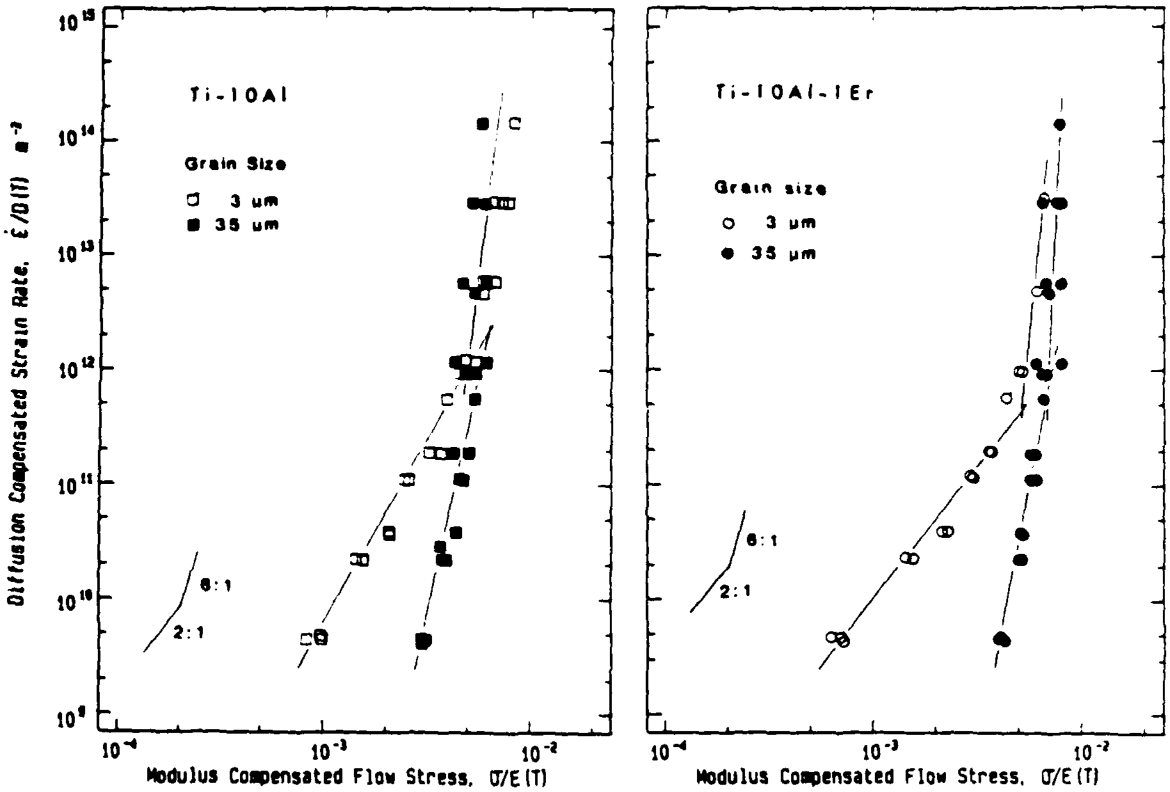

FIG. 10. Diffusion compensated near steady-state strain-rate as a function of modulus compensated flow stress for a.) Ti-10Al, and b.) Ti-10Al-1Er with grain sizes of 3 and 35 μm.

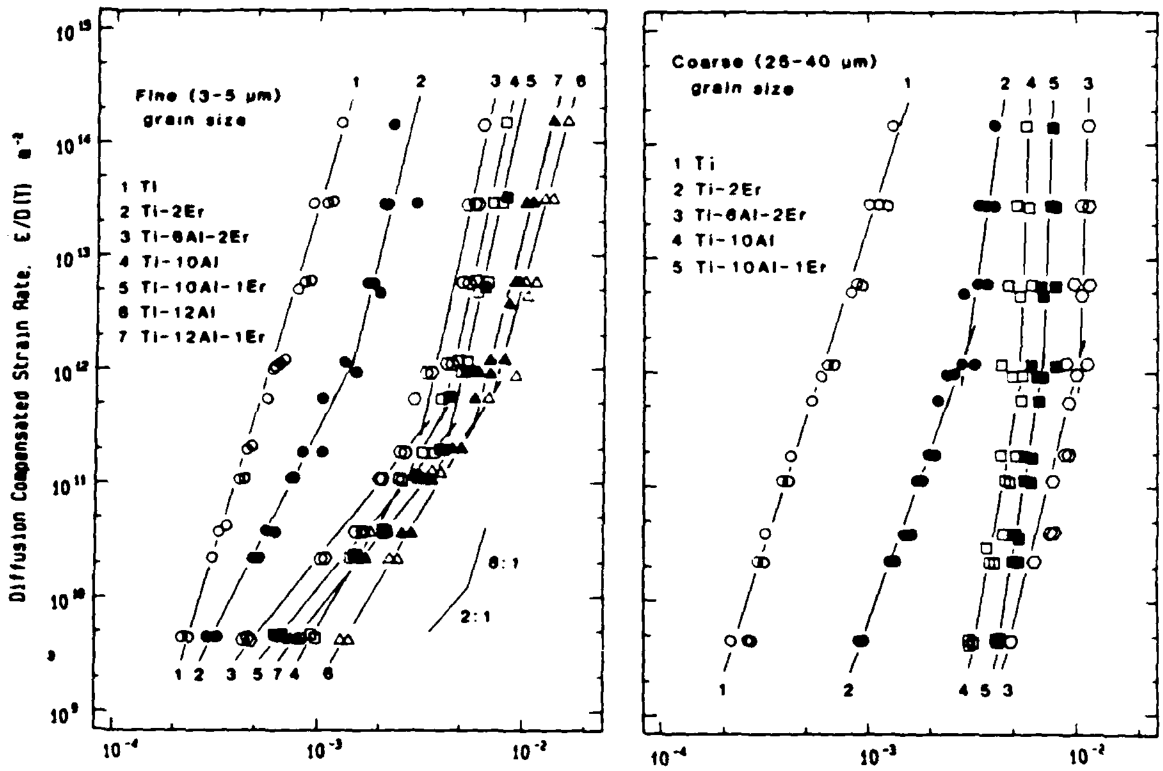

FIG. 11. Summary of results from alloys a.) in the as-processed, fine grained form, and b.) following grain growth anneals showing relative resistance to high temperature deformation.

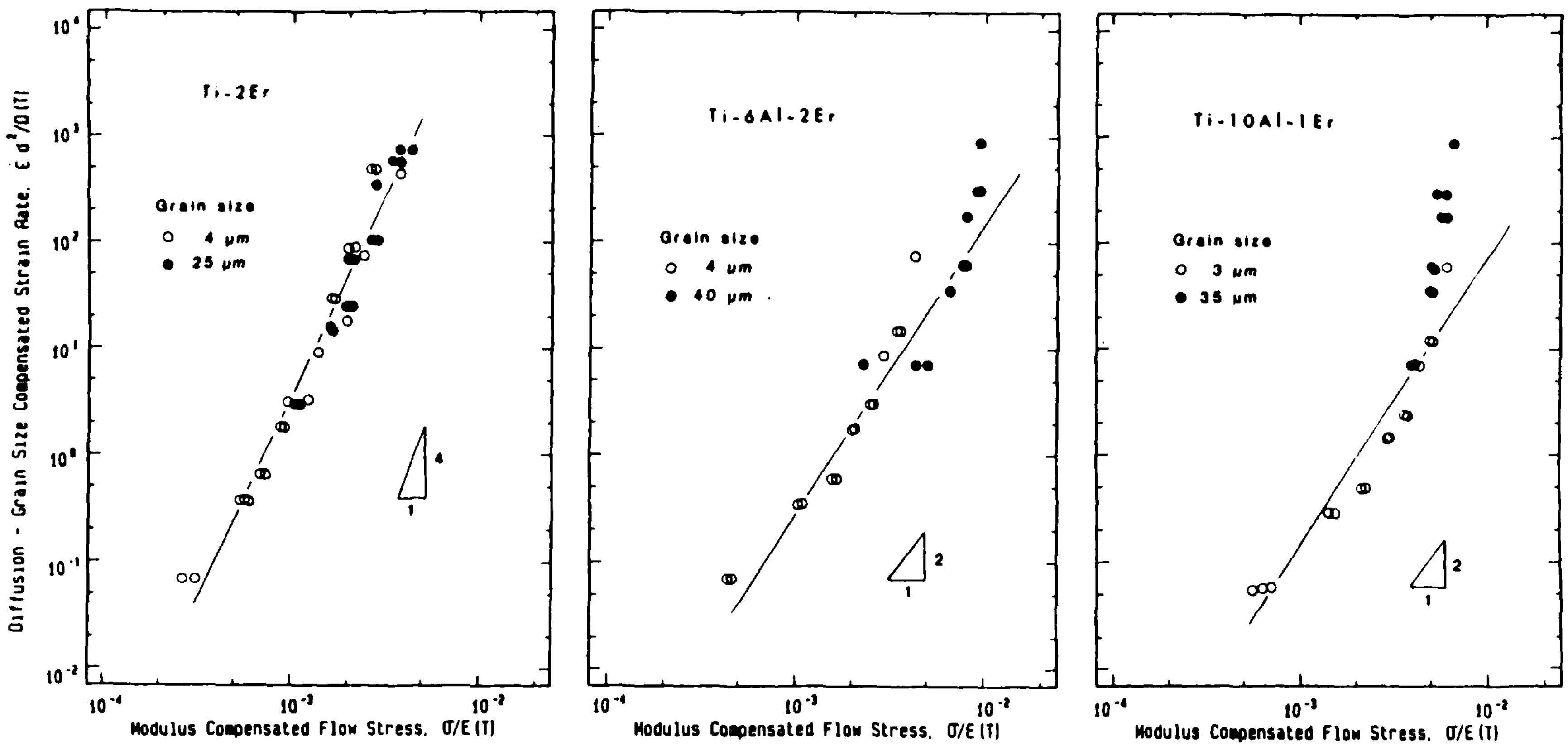

FIG. 12. Diffusion-grain size compensated strain-rate as a function of modulus compensated flow stress for a.) Ti-2Er, b.) Ti-6Al-2Er, and c.) Ti-10Al-1Er.

DATE
FILMED
5 8